NANO LETTERS

Letter

pubs.acs.org/NanoLett

Highly-Efficient Guiding of Motile Microtubules on Non-Topographical Motor Patterns

Cordula Reuther,[†,‡,⊥] Matthäus Mittasch,[†,‡,⊥] Sundar R. Naganathan,[‡,∥] Stephan W. Grill,[§,‡] and Stefan Diez*[,†,‡]

[†]B CUBE - Center for Molecular Bioengineering, Technische Universität Dresden, 01069 Dresden, Germany

[‡]Max Planck Institute of Molecular Cell Biology and Genetics, 01307 Dresden, Germany

[§]BIOTEC, Technische Universität Dresden, 01069 Dresden, Germany

Supporting Information

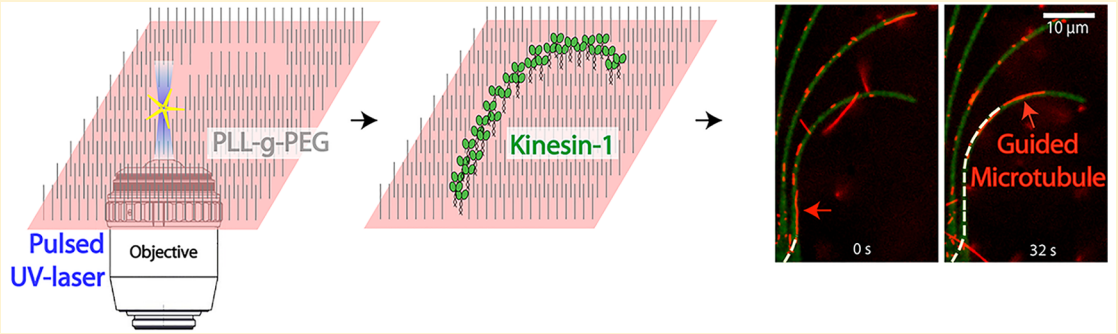

ABSTRACT: Molecular motors, highly efficient biological nanomachines, hold the potential to be employed for a wide range of nanotechnological applications. Toward this end, kinesin, dynein, or myosin motor proteins are commonly surface-immobilized within engineered environments in order to transport cargo attached to cytoskeletal filaments. Being able to flexibly control the direction of filament motion, and in particular on planar, non-topographical surfaces, has, however, remained challenging. Here, we demonstrate the applicability of a UV-laser-based ablation technique to programmably generate highly localized patterns of functional kinesin-1 motors with different shapes and sizes on PLL-*g*-PEG-coated polystyrene surfaces. Straight and curved motor tracks with widths of less than 500 nm could be generated in a highly reproducible manner and proved to reliably guide gliding microtubules. Though dependent on track curvature, the characteristic travel lengths of the microtubules on the tracks significantly exceeded earlier predictions. Moreover, we experimentally verified the performance of complex kinesin-1 patterns, recently designed by evolutionary algorithms for controlling the global directionality of microtubule motion on large-area substrates.

KEYWORDS: *Microtubules, kinesin, protein patterns, laser ablation, non-topographical guiding*

Molecular motors, driven by adenosine triphosphate (ATP), are envisioned to power novel devices for molecular detection, diagnostics, and biocomputation.[1−3] Thereby, the most promising manner of incorporating biomolecular systems into artificial environments is based on gliding motility assays: The motor proteins are immobilized on engineered surfaces to propel cytoskeletal filaments, which serve as carriers to specifically transport cargoes from one point to another.[4−7] For reaching the full potential of such hybrid-devices, the direction of the filament motion has to be controlled. In the past, topographical structures such as straight or complex-shaped channels coated with active motor proteins were used to spatially confine, guide,[8−10] or rectify the filament motion.[11] Furthermore, various approaches to spatially manipulate the filament motion by applying external forces, for example, flows,[12] electrical fields,[13] or magnetic fields,[14] were demonstrated. However, these techniques require either labor-intensive topographical surface modifications or well-defined external stimuli that cannot be easily generated in situ.

In contrast, chemical patterns of motor proteins attached nonuniformly to planar surfaces might increase the versatility of applications by combining flexible layouts, short fabrication times, and guiding without external signals. However, accomplishing reliable guiding is challenging. At pattern boundaries, filaments are only guided if the filament tip, which is fluctuating due to Brownian motion, is able to bend back onto the motor pattern. Thus, the guiding reliability decreases strongly with the angle at which the filaments approach the pattern boundary. One way for circumventing this limitation is to confine the range of approach angles by using

Received: June 20, 2017
Revised: August 18, 2017
Published: August 18, 2017

DOI: 10.1021/acs.nanolett.7b02606
Nano Lett. 2017, 17, 5699−5705

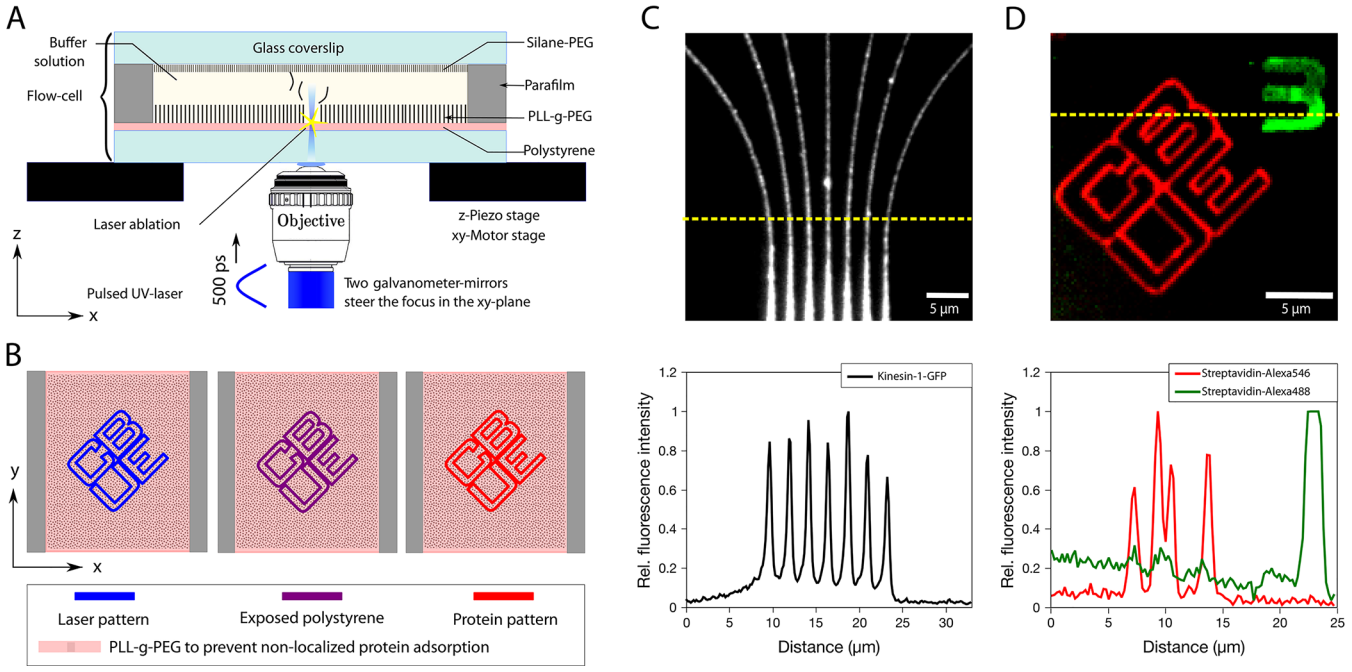

Figure 1. Generation of protein patterns by laser ablation. (A) Schematic of the experimental setup for laser ablation: The laser-focus was steered precisely along the bottom of the flow-cell in order to remove the protein-repellent PLL-*g*-PEG-coating. (B) Principle of surface modifications during the patterning process: A defined pattern was ablated on a homogeneous PLL-*g*-PEG-coating (left image) and led to polystyrene being exposed in the patterned area (middle image). Proteins bound out of solution exclusively onto the exposed polystyrene to form a protein pattern (right image). (C) Fluorescence image illustrating a nanopattern of GFP-labeled kinesin-1 molecules (upper image). The fluorescence intensity profile (lower image), determined along the yellow dotted line in the fluorescence image after subtracting the background intensity (measured prior to introducing the GFP-labeled kinesin-1 molecules) and by averaging over a width of five pixels, demonstrates a high contrast between patterned and blocked areas. (D) Color overlay of fluorescence images depicting sequentially generated patterns of streptavidin labeled with Alexa Fluor 546 (red) and Alexa Fluor 488 (green) (upper image). The fluorescence intensity profiles (lower image) along the dotted line in the color overlay (yellow) show a high specificity between the dual-color protein patterns.

narrow tracks as suggested by Clemmens et al.[8] Experimentally, this was verified for short kinesin-1 tracks[15,16] as well as for straight tracks of myosin II motor fragments (heavy meromyosin, HMM).[17] While guiding on kinesin-1 tracks was only limited by the length of the track (≤30 μm), on straight HMM tracks 60% of the actin filaments were guided longer than 20 μm, and 7% longer than 65 μm. Another way for increasing the transport efficiency is to optimize the chemical patterns according to computer simulations based on Brownian dynamics and genetic algorithms.[18] Patterns composed of narrow arc segments were predicted to lead to self-organized unidirectional filament transport. However, the success of both approaches will, among others, crucially depend on the capability of the utilized patterning technique. Toward this end, various general protein-patterning techniques based on optical lithography,[19,20] chemical vapor deposition,[21,22] atomic force microscopy,[23,24] and printing techniques[25] have been demonstrated recently. However, for all of these techniques there is a general trade-off between spatial resolution, throughput, maximum pattern size, and, very importantly though often less considered, the biological activity of the proteins on the patterns.

Here, we report on the programmable generation of arbitrarily shaped, functional motor protein patterns that facilitate the controlled motion of microtubules on planar surfaces. We applied a UV-laser-based ablation technique and explored the microtubule guiding performance on narrow kinesin-1 tracks. Moreover, we created kinesin-1 patterns composed of specifically arranged arc-lines to experimentally test the theoretically predicted directional transport of microtubules over large areas.

First, we chemically modified a substrate with a protein-repellent coating. Specifically, poly(L-lysine)-*g*-poly(ethylene glycol) (PLL-*g*-PEG) monolayers were coated electrostatically to plasma-activated polystyrene layers on glass substrates (see Methods). Then, for generating highly localized protein binding sites a diffraction-limited pulsed UV-laser,[26] coupled to a conventional inverted microscope,[27] was scanned along the PLL-*g*-PEG/polystyrene interface of the substrate (Figure 1A). Thereby, the protein-repellent PLL-*g*-PEG coating was plasma-oxidized in the irradiated areas. Consequently, the polystyrene surface became exposed and protein binding out of solution was enabled specifically to the ablated pattern (Figure 1B). Polystyrene layers were applied because after laser patterning they exhibit a smoother surface topography than glass (as was previously shown,[26] coinciding with our own obervations) and thus allow efficient protein adsorption. Moreover, to ensure maximal functionality of the patterned proteins, we adjusted the laser intensity such that the PLL-*g*-PEG coating was entirely removed, whereas the polystyrene layer was only superficially removed. The experiments illustrated in Figure 1C,D demonstrate our experimental approach: GFP-labeled kinesin-1 molecules were locally adsorbed onto a PLL-*g*-PEG surface along narrow tracks by incubating the protein solution after the laser-ablation process. Afterward excess proteins were washed out (Figure 1C). For streptavidin proteins labeled with two different fluorophores, Alexa Fluor 546 (red) and Alexa Fluor 488 (green), this process was performed by sequentially

DOI: 10.1021/acs.nanolett.7b02606
Nano Lett. 2017, 17, 5699−5705

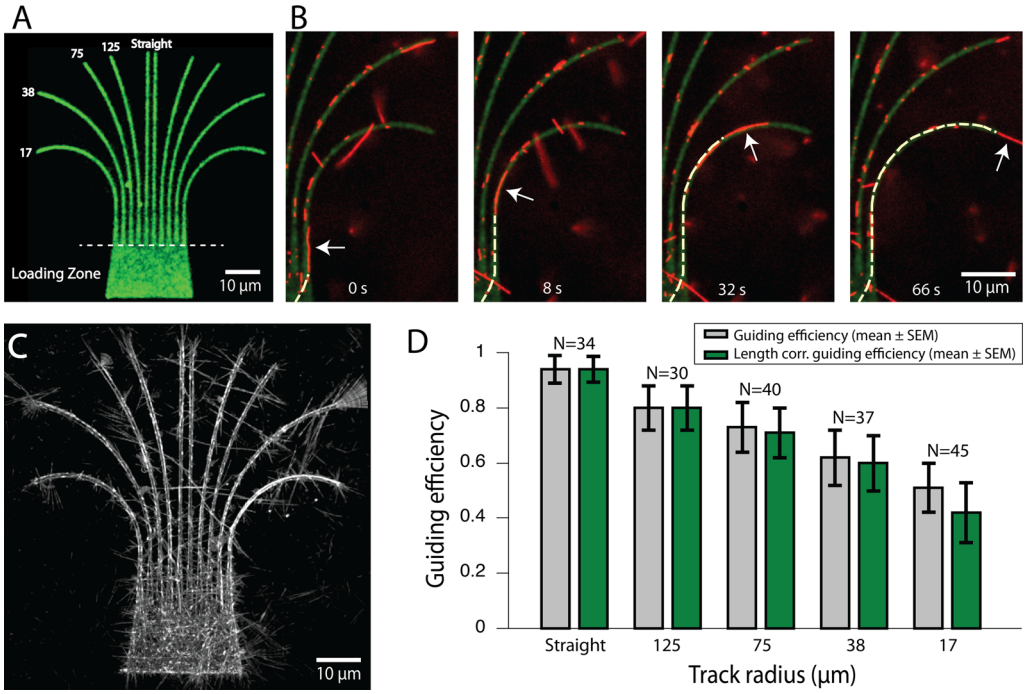

Figure 2. Guiding of gliding microtubules on straight and curved tracks patterned with kinesin-1 motor proteins. (A) Fluorescence image of the generated tracks (including a microtubule loading zone to increase the number of microtubules entering the tracks from one end) visualized by fluorescein-labeled casein. The numbers state the radius of the tracks in μm. (B) Microtubule guiding event on a track with a radius of 17 μm. Color overlay of fluorescence images showing microtubules (red) gliding along kinesin-1 tracks (green) and superimposed tracked microtubule pathways (yellow). (C) Maximum projection of microtubule motion on kinesin-1 tracks over a time period of 10 min. See also Movie S1. (D) The guiding efficiency (gray bars) for straight and curved tracks with different radii was determined as the number of microtubules following the track along its full length divided by the total number of microtubules that moved on the track starting from one end. The green bars show the guiding efficiencies corrected to the track length of the longest track.

incubating the respective protein solutions as well as washing excess proteins out after each of the two patterning steps (Figure 1D). The fluorescence image of the kinesin-1 pattern (Figure 1C), as well as the fluorescence intensity profile along the yellow dotted line show a high contrast between patterned and blocked surface areas. Moreover, the multicolor fluorescence image and the fluorescence intensity profiles of the dual-color streptavidin pattern (Figure 1D) demonstrate that a high contrast between two sequentially patterned proteins was achieved. The latter experiments thus displays the possibility of our approach for patterning different kinds of proteins side by side and in situ without the need of specific surface chemistry or prestructuring.

Next, we again generated narrow tracks of kinesin-1 motor proteins to study their potential for microtubule guiding, especially with respect to the curvature of the tracks. Because of its higher functionality, we now employed an unlabeled kinesin-1 motor construct. Using the described laser-based ablation approach, we created straight and curved tracks of different radii (17, 38, 75, and 125 μm) together with a microtubule loading zone to increase the number of microtubules entering the tracks from one end (Figure 2A). After laser ablation, we applied a casein solution containing a fraction of molecules labeled with fluorescein in order to visualize the pattern. After 5 min, the solution was exchanged for a kinesin-1 solution and the motor proteins were allowed to bind out of solution onto the casein-coated tracks. Finally, an ATP-containing motility solution with rhodamine-labeled microtubules was introduced. Microtubules frequently landed on the loading zone or on the tracks directly and started to move. Because of the processivity and flexibility of the kinesin-1 motors, the microtubules were able to use the tracks in any orientation. However, only few microtubules moved across the tracks whereas most microtubules followed the tracks and were guided along their length (Movie S1). Figure 2B shows an example of a microtubule guiding event on a kinesin-1 track with a radius of 17 μm. Moreover, microtubules exclusively translocated on the patterns verifying efficient blocking of the surface areas around (Figure 2C). We quantified the guiding efficiencies (GE) for straight and curved tracks with different radii by determining the number of microtubules following the tracks along their full lengths divided by the total number of microtubules that moved on the tracks starting from one end (i.e., microtubules landing in the middle of the tracks were disregarded). To account for the slightly different lengths L_{track} of the patterned tracks (56.3, 56.3, 56.0, 55.7, and 44.8 μm for radii of ∞, 125, 75, 38, and 17 μm, respectively), we subsequently corrected the guiding efficiencies for each radius by multiplying GE with the ratio of L_{track} devided by the length of the longest track. While guiding on straight tracks proved to be highly reliable (GE = 94%), the guiding efficiency reduced with increasing track curvature. This behavior was expected because increasing track curvature increased the likelihood of steeper approach angles of the microtubules with the boundaries, enhancing the track leavage probability and thus reducing the guiding distances. However, even on the tracks with the highest curvature (radius = 17 μm) still 60% of the microtubules moved over distances as long as 45 μm, that is, the full track length. We then determined the characteristic travel distance λ for a given track with length L_{track} and radius R by $\lambda_R = -\frac{L_{track}}{\ln(GE)}$, assuming an exponential

DOI: 10.1021/acs.nanolett.7b02606
Nano Lett. 2017, 17, 5699−5705

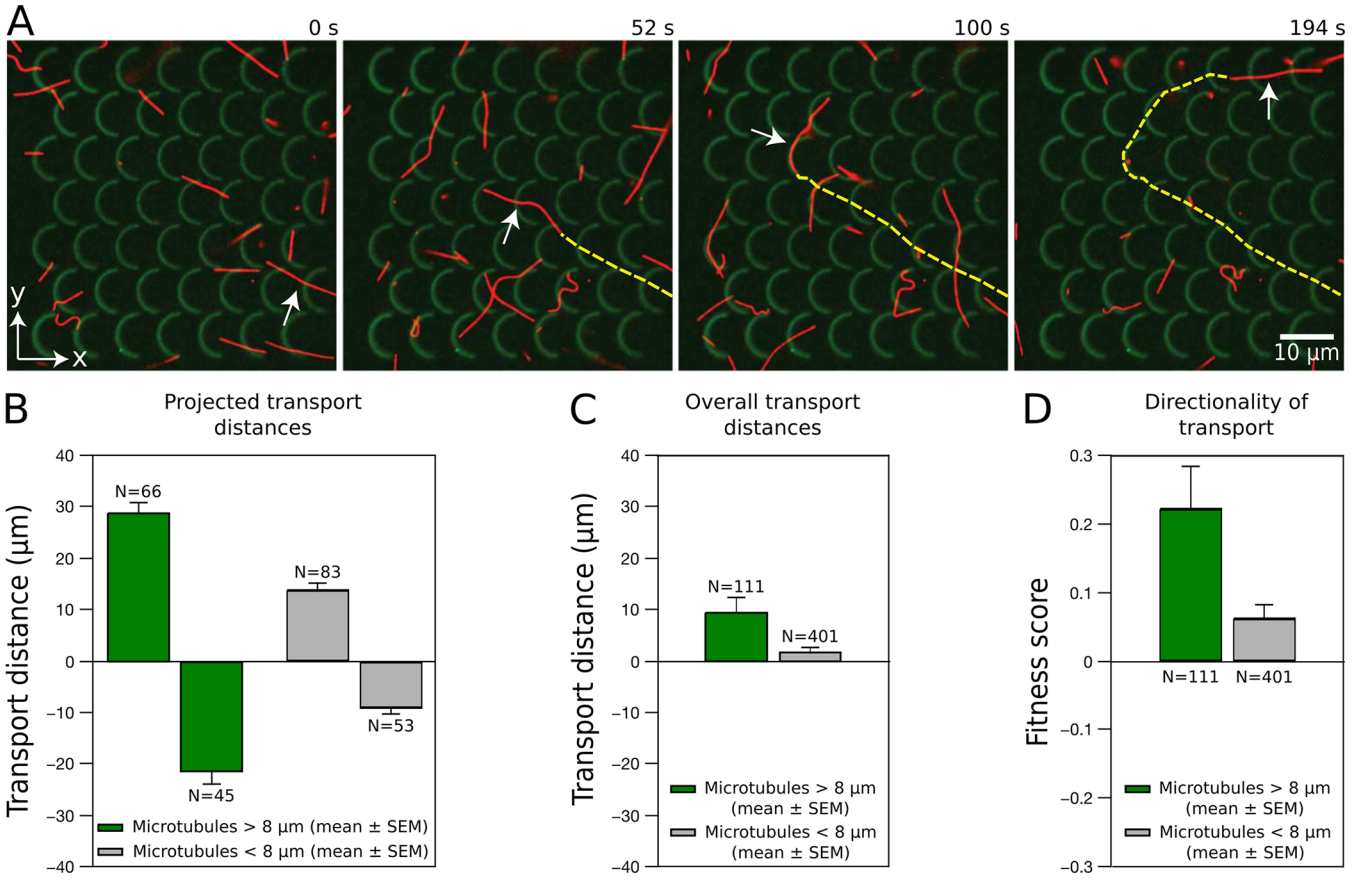

Figure 3. Global direction of gliding microtubules on a periodic pattern of kinesin-1 motors. (A) Periodically arranged arc-segments (similar to the ones recently simulated and optimized for directional microtubule transport by Rupp and Nedelec[18]) were generated within a 60 μm × 60 μm large area. The fluorescence images show overlays of microtubules (red) that are transported on the kinesin-1 pattern (green; visualized using fluorescein-labeled casein). As an example, one tracked microtubule-path is indicated (yellow dashed line, see also Movie S2). (B) Projected transport distances (Δx) of the microtubule paths. For long microtubules (length >8 μm) gliding in positive x-direction we found Δx to be increased by 35% compared to microtubules gliding in negative x-direction. Short microtubules (length <8 μm) only moved short distances in either direction or followed exactly the contour of an arc ($\Delta x = 0$, $n = 265$). (C) Combined projected transport distances for both directions. Short microtubules exhibited an about 80% reduced overall transport distance compared to long microtubules. (D) Averaged experimental fitness scores of the microtubule paths as a measure for the degree of transport directionality. For long microtubules we obtained $f = 0.22 \pm 0.06$ ($n = 111$), indicating a clear preference of motion into the desired direction, whereas for short microtubules $f = 0.056 \pm 0.018$ ($n = 401$) indicated an almost random motion.

decay of the guiding efficiency with respect to the actual distance traveled on a track. We obtained characteristic travel distances of about 930, 250, 170, 115, and 70 μm for tracks with radii of ∞, 125, 75, 38, and 17 μm, respectively.

The lateral widths of the tracks were quantitatively estimated by measuring the fluorescence intensity profiles perpendicular to the long axes of the tracks. Fitting these intensity profiles by a Gaussian function yielded an apparent width (full width at half-maximum) of $w_{app} = 650 \pm 130$ nm (mean ± standard deviation, $n = 14$). Because of the limited optical resolution, this value represents the convolution of the real track width w_{track} with the one-dimensional point-spread-function (width w_{PSF}) of our imaging system. The real track width can thus be estimated by $w_{track} = \sqrt{w_{app}^2 - w_{PSF}^2}$ (deconvolution of two Gaussian functions[28]). Because the lateral width of a microtubule is at least 10 times smaller than the optical resolution of the imaging system, it is reasonable to approximate w_{PSF} by measuring the fluorescence intensity profile perpendicular to an Alexa 488-labeled reference microtubule. Such a measurement yielded 500 ± 40 nm ($n = 9$) and the actual lateral width of the generated track was thus determined to be $w_{track} = 420 \pm 210$ nm. These results clearly show that restricting microtubules to shallow approach angles by narrowing the track width opens up a great potential for non-topographical guiding (as previously hypothesized by Clemmens et al.[8]). Compared to a predicted average travel distance of only 35 μm for straight chemical tracks with a width of 1.5 μm,[8] the kinesin-1 tracks reported here are capable of reliably transporting cargo over distances in the range of one millimeter.

Toward controlling filament motion within molecular devices on a global scale, we tested the experimental performance of a simulated pattern which was composed of motor proteins arranged in periodically repeating arc segments. Given that all ends of the arc segments are pointing into the same direction, such patterns were recently predicted by Rupp and Nedelec to lead to highly efficient directional filament transport,[18] the underlying mechanism being based on asymmetric progressive deflection as well as occasional short guiding events. Figure 3A shows a kinesin-1 pattern of periodically arranged arc-segments (half-circles with a diameter of 8 μm, laterally offset by 8 μm in each row) based on a geometry extracted from the simulation[18] and experimentally generatd by the procedure as described above. The patterned area was 60 μm × 60 μm in size and

DOI: 10.1021/acs.nanolett.7b02606
Nano Lett. 2017, 17, 5699−5705

contained seven rows each with seven arc segments. In order to get more microtubules moving either from the right or the left side across the pattern (instead of landing somewhere in the middle), we additionally added rectangular areas as landing zones on both sides (not shown). Microtubules glided exclusively on the generated pattern and detached from the surface when they reached a boundary (Movie S2). We tracked all microtubule paths using the segmented line tool in ImageJ and evaluated their directionality when moving over the pattern. The analysis of 512 microtubule paths revealed a dependence on microtubule length: Long microtubules (microtubule length >8 μm, that is, longer than the lateral offset of the arc segments) were able to move over long distances in both directions across the pattern whereas short microtubules (microtubule length <8 μm) mainly followed the contours of the arcs and often detached from the pattern after short distances.

Evaluating the projected transport distances $\Delta x = x2 - x1$ of the paths, with $x1$ and $x2$ being the x-coordinates of the beginning and the end of the path, we found for long microtubules that Δx was 28.6 ± 2.1 μm (mean ± SEM, n = 66) when gliding into the desired direction (that is, the direction the ends of the arcs were pointing to) and −21.3 ± 2.5 μm (mean ± SEM, n = 45) when gliding in the opposite direction. In total, 60% of the long microtubules were traveling into the desired direction with projected transport distances about 35% higher than in the opposite direction (Figure 3B). This finding was in agreement with the observation that microtubules moving against the desired direction were often redirected, similar to the example microtubule marked in Figure 3A. For the short microtubules Δx was 13.5 ± 1.3 μm (mean ± SEM, n = 83) and −8.9 ± 1.2 μm (mean ± SEM, n = 53) when gliding short distances into the desired and the opposite direction (Figure 3B). Additionally, Δx was zero (n = 265) for short microtubules that moved exactly along the contour of just one arc segment before detachment. When combining the projected transport distances for both directions, we obtained 9.6 ± 2.8 μm (n = 111) for the long microtubules and 1.62 ± 0.46 μm (mean ± SEM, n = 401) for the short microtubules. Thus, short microtubules exhibited an about 80% reduced overall transport distance (Figure 3C).

In order to compare our results with the simulation we determined the fitness score $f = \Delta x/L$ for each individual gliding event, with L being the full length of the nonprojected microtubule path. In the genetic algorithm used by Rupp and Nedelec for optimizing the patterns, the fitness score was the key parameter to evaluate their performance. In general, f can be between −1 and +1, the actual value indicating the degree of directionality: f = 1 corresponds to a microtubule moving straight into the positive x-direction (desired direction) and f = −1 corresponds to a microtubule moving straight into the negative x-direction (nondesired direction). For f = 0, there would be no net transport into any direction. When averaging the experimental fitness scores for short and long microtubules separately, we obtained f = 0.056 ± 0.018 (mean ± SEM, n = 401) for the short microtubules, indicating an almost random motion (Figure 3D). However, motion of the long microtubules revealed f = 0.22 ± 0.06 (n = 111), indicating a clear preference of motion into the desired direction. This finding qualitatively agrees with the predictions and additionally implies a length sorting mechanism of the pattern. Only long microtubules are transported in a directional manner, whereas short microtubules glide randomly and detach from the surface, when they do not have the length to bridge the gap from one arc to the next.

Although we experimentally observed a directionality for the motion of long microtubules across the arc-pattern, in the simulation the pattern performed better by reaching a fitness score of f = 0.77 ± 0.01 (ref 18). We believe there are multiple reasons for this discrepancy: (i) One major point is the limited size of the experimental pattern in contrast to an infinitely large pattern in the simulation. The larger the pattern is, the higher is the probability for a microtubule to get deflected toward the desired direction. In the experiment, we often observed that microtubules initially moving into the nondesired direction were redirected but detached from the surface at the bottom or the top border of the pattern before Δx reached positive values. (ii) Besides the pattern size, simplifications in the simulation might also contribute to the difference in the fitness scores. For instance, in the simulations the arc-pattern was composed of infinitesimal narrow tracks of motor proteins, which might have overperformed with regard to the guiding efficiency. Hence, reducing the experimental track width may improve the performance. (iii) Another crucial factor determining the pattern performance is the density of active motor proteins on the track. The assumed density of motor proteins in the simulation (10 motors per micrometer track length) might have been overestimated. (iv) Even more importantly, dysfunctional motor proteins were not considered in the simulations but cannot be completely avoided during the complex experimental procedures. However, active and complex motor protein patterns, such as reported here, have so far not been demonstrated using alternative patterning techniques, for example, electron beam lithography[29] or AFM-based nanoshaving.[24]

We used a UV-laser-based ablation technique to realize complex user-defined patterns of active motor proteins on planar surfaces. We experimentally demonstrated that straight, and for the first time also curved, tracks of the motor protein kinesin-1 (possessing track widths of less than 500 nm) were able to reliably guide microtubules. The guiding efficiency was curvature dependent but the characteristic travel lengths of the microtubules by far exceeded earlier reports and predictions. Thus, the presented results may open up new routes toward controlling microtubule motion in self-organized hybrid-devices. In this regard, screening for optimized local and global track geometries with the help of computer simulations, for example, by applying an evolutionary design method as presented by Sunagawa et al.,[30] will be very useful. The geometries recently simulated by Rupp and Nedelec[18] already provided an excellent foundation for testing if the global microtubule motion can be experimentally biased into a desired direction. When reproducing one of these patterns with arc-like kinesin-1 motor tracks we indeed observed the global steering of long microtubules into the desired direction. In the future, patterning of different types of motor proteins, for example, kinesin-1 and cytoplasmic dynein, next to each other could be used to solve more complex functions. Thereby, arrays of tasks such as the rectifying and reliable sorting of filaments with different lengths in combination with cargo delivery at detection zones[31] could be realized to achieve the full applicability of motor-powered molecular detection devices. Furthermore, we foresee a large potential of the patterning approach to design well-defined and reproducible biophysical experiments to study multimotor transport systems.

DOI: 10.1021/acs.nanolett.7b02606
Nano Lett. 2017, 17, 5699−5705

Methods. *Protein-Repellent Surface Coatings.* Glass coverslips (22 × 22 mm^2, Corning) were cleaned by sonication in Mucasol/water (1:20; v = (v) for 15 min followed by rinsing in deionized water for 2 min. Further, coverslips were sonicated in ethanol/water (1:1; v = (v) for 10 min, rinsed in deionized water for 2 min, rinsed in Milli-Q-water for 2 min and finally dried using a nitrogen airflow. Then, coverslips were spin-coated for 30 s at 3000 rpm with adhesion promoter Ti-prime (Microchemicals), baked for 2 min at 120 °C and spin-coated for 30 s at 3000 rpm with 0.5% polystyrene solution (Sigma-Aldrich, Germany) in toluene (VWR, Germany). Directly after the oxygen plasma treatment (FEMTO, Diener Electronics, Germany) for 6 s at 60% radio frequency power, the now negatively charged polystyrene coated coverslips were incubated with 0.1 mg/mL PLL-*g*-PEG (SuSoS AG, Switzerland) in 100 mM HEPES, pH = 7.4, at room temperature for 1 h on a parafilm (Pechiney, U.S.A.) surface within a humid box. Finally, the coverslips were lifted off slowly and gentle nitrogen airflow was used to ensure complete PLL-*g*-PEG solution dewetting.

Laser Patterning. The experiments were performed in 3 mm wide flow-cells consisting of a glass coverslip (22 × 22 mm^2) coated with PLL-*g*-PEG for the bottom, a (18 × 18 mm^2) PEGylated coverslip[32] for the top and two stripes of parafilm as spacers. For the patterning process, a self-built setup was used,[27] which was based on a passively Q-switched, third-harmonic ND:YAG laser (PowerCHIP, JDS Uniphase) with a wavelength of 355 nm in the UV spectral range, a pulse energy of up to 10 μJ and a pulse duration of 500 ps (leading to peak power densities of up to 10 TW/cm^2). The laser unit was implemented on an inverted Zeiss Axio Observer Z1 microscope (Zeiss, Germany) equipped with a 63× water immersion objective C-Apochromat NA of 1.2 (Zeiss, Germany) and a piezo-electric positioner to correct for chromatic aberrations due to the use of UV-light. Patterns were generated by scanning the laser beam along the flow-cell surface using a scan-head LDS-10-OH (GSI, U.S.A.). The latter consisted of two galvanometric mirrors that deviated the laser beam in two perpendicular axis independently across a scanning field of 80 × 80 μm^2 with a steering accuracy of 30 nm. The pattern was filled with a density of 4 spots/μm, whereas each spot was exposed with five pulses at a repetition rate of 1 kHz. The laser intensity was set to 30% of the minimum visible effect of pulsed UV laser-glass interaction which corresponds to about 0.4 μJ deposited in the medium, or 65 GW/cm^2 of peak power density threshold. Therefore, unblocked regions were generated. For the experiments depicted in Figure 1, kinesin-1-GFP (10 μg/mL in BRB80 with 0.5 mg/mL casein, 1 mM ATP as well as 10 mM dithiothreitol; construct described below) and streptavidin proteins labeled with Alexa Fluor 546 (0.25 mg/mL in BRB80), respectively, were adsorbed out of solution. After 10 min unbound proteins were washed out. In Figure 1D, a second pattern was generated, followed by incubation of a solution containing streptavidin proteins labeled with Alexa Fluor 488 (0.25 mg/mL in BRB80). Again, the streptavidin proteins were allowed to adsorb out of solution for 10 min and subsequently the unbound streptavidin proteins were washed out thoroughly. Finally, fluorescence image acquisition was performed.

Kinesin-1 Gliding Motility Experiments. Microtubules were polymerized from 5 μL of rhodamine-labeled porcine brain tubulin[33] in BRB80 (80 mM PIPES, adjusted to pH = 6.9 with KOH, 1 mM EGTA, 1 mM $MgCl_2$) with 5 mM $MgCl_2$, 1 mM GTP, 5% DMSO at 37 °C for 30 min. The microtubules were stabilized and diluted 100-fold in BRB80 containing 10 μM Taxol. Full-length *Drosophila melanogaster* kinesin-1 motor molecules (with and without GFP) were expressed in insect cells and purified applying published protocols.[34] Gliding assays were prepared after completing the laser patterning process and rinsing the flow-cell with 60 μL of BRB80. A solution containing casein (0.4 mg/mL) as well as fluorescein-labeled casein (0.1 mg/mL) was perfused into the flow-cell and allowed to adsorb to the exposed surface for 5 min. This solution was exchanged for a 10 μg/mL kinesin-1 solution in BRB80 with 0.2 mg/mL casein, 1 mM ATP as well as 10 mM dithiothreitol and incubated for 5 min. A BRB80 solution containing 10 μM Taxol, 1 mM ATP, 40 mM D-glucose, 55 μg/mL glucose oxidase, 11 mg/mL catalase and 10 mM dithiothreitol was added to the flow-cell. After the motor-patterns had been localized, a BRB80 solution containing microtubules (580 nM), 10 μM Taxol, 1 mM ATP, 40 mM D-glucose, 55 μg/mL glucose oxidase, 11 mg/mL catalase, and 10 mM dithiothreitol was flown in.

Imaging. Image acquisiton was performed using an inverted fluorescence microscope Zeiss Axiovert 200 M (Zeiss, Germany) with a 100× oil immersion objective Plan-Neofluar NA = 1.3 (Zeiss, Germany). For excitation, a Lumen 200 metal arc lamp (Prior Scientific Instruments, U.S.A.) was applied. The data was recorded with an electron multiplying charge-coupled device (EMCCD) camera (iXon + EMCCD, DU-897E, Andor) having a pixel size of 16 μm. If not stated differently, images were acquired every 2 s with an exposure time of 100 ms using MetaMorph (Molecular Devices, U.S.A.).

■ ASSOCIATED CONTENT

Supporting Information

The Supporting Information is available free of charge on the ACS Publications website at DOI: 10.1021/acs.nanolett.7b02606.

Complete descriptions of movies (PDF)

Timelapse movie of microtubule motility along non-topographical kinesin-1 tracks with different curvatures (AVI)

Timelapse movie of microtubule motility on a periodic pattern of kinesin-1 arc segments (AVI)

■ AUTHOR INFORMATION

Corresponding Author

*E-mail: stefan.diez@tu-dresden.de. Phone: +49 351 46343010.

ORCID

Stefan Diez: 0000-0002-0750-8515

Present Address

∥(S.R.N.) The Francis Crick Institute, 1 Midland Road, London NW1 1AT, United Kingdom.

Author Contributions

⊥C.R. and M.M. contributed equally.

Notes

The authors declare no competing financial interest.

■ ACKNOWLEDGMENTS

The authors would like to thank Corina Bräuer for technical support, Manuel Thery for fruitful discussion on the implementation of the experimental methodology and Till Korten for comments on the manuscript. The work was

DOI: 10.1021/acs.nanolett.7b02606
Nano Lett. 2017, 17, 5699−5705

financially supported by the European Research Council (starting Grant 242933), the European Union (Grant Agreements 613044 ABACUS and 732482 Bio4Comp), the Volkswagen Foundation (Grant I/82093), as well as the German Research Foundation (DFG) within the Cluster of Excellence Center for Advancing Electronics Dresden.

REFERENCES

(1) Agarwal, A.; Hess, H. *Prog. Polym. Sci.* **2010**, *35*, 252−277.
(2) Korten, T.; Mansson, A.; Diez, S. *Curr. Opin. Biotechnol.* **2010**, *21*, 477−488.
(3) Nicolau, D. V.; Lard, M.; Korten, T.; van Delft, F. C. M. J. M.; Persson, M.; Bengtsson, E.; Mansson, A.; Diez, S.; Linke, H.; Nicolau, D. V. *Proc. Natl. Acad. Sci. U. S. A.* **2016**, *113*, 2591−2596.
(4) Brunner, C.; Wahnes, C.; Vogel, V. *Lab Chip* **2007**, *7*, 1263−1271.
(5) Lin, C.-T.; Kao, M.-T.; Kurabayashi, K.; Meyhofer, E. *Nano Lett.* **2008**, *8*, 1041−1046.
(6) Bachand, G. D.; Hess, H.; Ratna, B.; Satir, P.; Vogel, V. *Lab Chip* **2009**, *9*, 1661−1666.
(7) Fischer, T.; Agarwal, A.; Hess, H. *Nat. Nanotechnol.* **2009**, *4*, 162−166.
(8) Clemmens, J.; Hess, H.; Lipscomb, R.; Hanein, Y.; Böhringer, K. F.; Matzke, C. M.; Bachand, G. D.; Bunker, B. C.; Vogel, V. *Langmuir* **2003**, *19*, 10967−10974.
(9) Hess, H.; Matzke, C. M.; Doot, R. K.; Clemmens, J.; Bachand, G. D.; Bunker, B. C.; Vogel, V. *Nano Lett.* **2003**, *3*, 1651−1655.
(10) Dennis, J. R.; Howard, J.; Vogel, V. *Nanotechnology* **1999**, *10*, 232−236.
(11) van den Heuvel, M. G. L.; Butcher, C. T.; Smeets, R. M. M.; Diez, S.; Dekker, C. *Nano Lett.* **2005**, *5*, 1117−1122.
(12) Stracke, R.; Böhm, K. J.; Burgold, J.; Schacht, H.-J.; Unger, E. *Nanotechnology* **2000**, *11*, 52.
(13) van den Heuvel, M. G. L.; de Graaff, M. P.; Dekker, C. *Science* **2006**, *312*, 910−914.
(14) Bras, W.; Diakun, G. P.; Díaz, J. F.; Maret, G.; Kramer, H.; Bordas, J.; Medrano, F. J. *Biophys. J.* **1998**, *74*, 1509−1521.
(15) Reuther, C.; Hajdo, L.; Tucker, R.; Kasprzak, A. A.; Diez, S. *Nano Lett.* **2006**, *6*, 2177−2183.
(16) Bhagawati, M.; Ghosh, S.; Reichel, A.; Froehner, K.; Surrey, T.; Piehler, J. *Angew. Chem., Int. Ed.* **2009**, *48*, 9188−9191.
(17) Sundberg, M.; Bunk, R.; Albet-Torres, N.; Kvennefors, A.; Persson, F.; Montelius, L.; Nicholls, I. A.; Ghatnekar-Nilsson, S.; Omling, P.; Tagerud, S.; Mansson, A. *Langmuir* **2006**, *22*, 7286−7295.
(18) Rupp, B.; Nedelec, F. *Lab Chip* **2012**, *12*, 4903−4910.
(19) Yamaguchi, M.; Nishimura, O.; Lim, S. H.; Shimokawa, K.; Tamura, T.; Suzuki, M. *Colloids Surf., A* **2006**, *284-285*, 532−534.
(20) Allen, R. D. *J. Photopolym. Sci. Technol.* **2007**, *20*, 453−455.
(21) Slocik, J. M.; Beckel, E. R.; Jiang, H.; Enlow, J. O.; Zabinski, J. S.; Bunning, T. J.; Naik, R. R. *Adv. Mater.* **2006**, *18*, 2095−2100.
(22) Jung, J. M.; Kwon, K. Y.; Ha, T. H.; Chung, B. H.; Jung, H. T. *Small* **2006**, *2*, 1010−1015.
(23) Ginger, D. S.; Zhang, H.; Mirkin, C. A. *Angew. Chem., Int. Ed.* **2004**, *43*, 30−45.
(24) Tinazli, A.; Piehler, J.; Beuttler, M.; Guckenberger, R.; Tampe, R. *Nat. Nanotechnol.* **2007**, *2*, 220−225.
(25) Xia, Y. N.; Whitesides, G. M. *Annu. Rev. Mater. Sci.* **1998**, *28*, 153−184.
(26) Vignaud, T.; Galland, R.; Tseng, Q. Z.; Blanchoin, L.; Colombelli, J.; Thery, M. *J. Cell Sci.* **2012**, *125*, 2134−2140.
(27) Colombelli, J.; Grill, S. W.; Stelzer, E. H. K. *Rev. Sci. Instrum.* **2004**, *75*, 2773−2773.
(28) Bracewell, R. *Fourier Transform and Its Applications* **1999**, *25−50*, 243−244.
(29) Zhang, G. J.; Tanii, T.; Zako, T.; Hosaka, T.; Miyake, T.; Kanari, Y.; Funatsu, T.; Ohdomari, I. *Small* **2005**, *1*, 833−837.
(30) Sunagawa, T.; Tanahashi, A.; Downs, M. E.; Hess, H.; Nitta, T. *Lab Chip* **2013**, *13*, 2827−2833.
(31) Schmidt, C.; Vogel, V. *Lab Chip* **2010**, *10*, 2195−2198.
(32) Papra, A.; Gadegaard, N.; Larsen, N. B. *Langmuir* **2001**, *17*, 1457−1460.
(33) Castoldi, M.; Popov, A. V. *Protein Expression Purif.* **2003**, *32*, 83−88.
(34) Korten, T.; Chaudhuri, S.; Tavkin, E.; Braun, M.; Diez, S. *IEEE Trans. NanoBiosci.* **2016**, *15*, 62−69.

DOI: 10.1021/acs.nanolett.7b02606
Nano Lett. 2017, 17, 5699−5705